


SCIENTIFIC REPORTS



OPEN

The photocycle of orange carotenoid protein conceals distinct intermediates and asynchronous changes in the carotenoid and protein components

E. G. Maksimov¹, N. N. Sluchanko^{1,2}, Y. B. Slonimskiy^{2,3}, E. A. Slutskaia⁴, A. V. Stepanov⁴, A. M. Argentova-Stevens⁴, E. A. Shirshin⁵, G. V. Tsoraev¹, K. E. Klementiev¹, O. V. Slatinskaya¹, E. P. Lukashev¹, T. Friedrich⁶ , V. Z. Paschenko¹ & A. B. Rubin¹

The 35-kDa Orange Carotenoid Protein (OCP) is responsible for photoprotection in cyanobacteria. It acts as a light intensity sensor and efficient quencher of phycobilisome excitation. Photoactivation triggers large-scale conformational rearrangements to convert OCP from the orange OCP^O state to the red active signaling state, OCP^R, as demonstrated by various structural methods. Such rearrangements imply a complete, yet reversible separation of structural domains and translocation of the carotenoid. Recently, dynamic crystallography of OCP^O suggested the existence of photocycle intermediates with small-scale rearrangements that may trigger further transitions. In this study, we took advantage of single 7 ns laser pulses to study carotenoid absorption transients in OCP on the time-scale from 100 ns to 10 s, which allowed us to detect a red intermediate state preceding the red signaling state, OCP^R. In addition, time-resolved fluorescence spectroscopy and the assignment of carotenoid-induced quenching of different tryptophan residues derived thereof revealed a novel orange intermediate state, which appears during the relaxation of photoactivated OCP^R to OCP^O. Our results show asynchronous changes between the carotenoid- and protein-associated kinetic components in a refined mechanistic model of the OCP photocycle, but also introduce new kinetic signatures for future studies of OCP photoactivity and photoprotection.

The 35-kDa Orange Carotenoid Protein (OCP) utilizes the extraordinary capability of its carotenoid cofactor to convert electronic excitation energy by internal conversion within a few picoseconds into harmless heat in order to shield the sensitive photosystems from excessive excitation energy arriving from the phycobilisome (PBs) antennae complexes at high light intensities^{1–9}. OCP is a blue-green light photoreceptor capable of undergoing a red shift of its absorption spectrum upon illumination^{10,11}. Photoactivity necessarily requires a single 4-ketolated carotenoid molecule to be coordinated by OCP, which is 3'-hydroxyechinenone when purified from cyanobacteria^{3,12}, but also incorporation of echinenone (4-keto; ECN) and the 4,4'-diketolated canthaxanthin (CAN) preserves photoactivity, whereas binding of the 3,3'-dihydroxylated zeaxanthin precludes spectral switching^{13–15}. OCP is divided into two domains of about half its molecular weight, with an all- α -helical N-terminal domain (NTD) and a mixed α/β -type C-terminal domain (CTD) bearing similarity to the NTF-2 protein family of nuclear transfer factors (Pfam: PF02136), which almost symmetrically enclose a central carotenoid-binding

¹Lomonosov Moscow State University, Department of Biophysics, Faculty of Biology, 119991, Moscow, Russia.

²A.N. Bach Institute of Biochemistry, Federal Research Center of Biotechnology of the Russian Academy of Sciences, 119071, Moscow, Russia. ³Lomonosov Moscow State University, Department of Biochemistry, Faculty of Biology, 119991, Moscow, Russia. ⁴M.M. Shemyakin and Yu.A. Ovchinnikov Institute of Bioorganic Chemistry, Russian Academy of Sciences, Miklukho-Maklaya Str., 16/10, Moscow, 117997, Russia. ⁵Lomonosov Moscow State University, Department of Quantum Electronics, Faculty of Physics, Moscow, 119992, Russia. ⁶Technical University of Berlin, Institute of Chemistry PC 14, Straße des 17. Juni 135, D-10623, Berlin, Germany. Correspondence and requests for materials should be addressed to E.G.M. (email: emaksimoff@yandex.ru)

cavity that nearly completely shields the cofactor from the aqueous environment^{16,17}. The orange state OCP^O is structurally stabilized by distinct carotenoid-protein interactions including specific H-bonds from Trp-288 and Tyr-201 in the CTD (amino acid numbering refers to OCP from *Synechocystis* sp. PCC 6803) to the 4-keto oxygen at one of the β -rings, as well as interactions to Tyr-44 and π -stacking with Trp-110 in the NTD, but also extensive protein-protein interactions involving multiple H-bonds across the extensive NTD-CTD inter-domain interface (including two formed between Asn-104 and Trp-277, and Arg-155 and Glu-244¹⁸) and binding of the α A-helix of the N-terminal extension (NTE) to the central β -sheet surface on the CTD^{19–22}.

Upon photoconversion from the orange OCP^O state, the red-shifted OCP^R state is formed, which can interact with phycobilisome antennae complexes and quenches their fluorescence in the photoprotective mechanism of non-photochemical quenching^{7,21,23,24}. According to biochemical (size-exclusion chromatography, SEC) and structural (small-angle X-ray scattering, SAXS, or static and dynamic X-ray crystallography) studies, the active, quenching OCP^R state is characterized by increased disorder in terms of a molten globule, detachment and unfolding of the α A-helix from the CTD, domain separation, and, eventually, a carotenoid translocation by 12 Å into the NTD, thereby forming a spectral state indistinguishable from the one of the Red Carotenoid Protein (RCP). The latter is a hydrolysis product of OCP comprising only the carotenoid-bound N-terminal domain, which constitutively quenches PBs fluorescence^{25–28}. The photoprotective mechanism *in vivo* is terminated by the Fluorescence Recovery Protein (FRP), which promotes dissociation of OCP^R from the PBs and accelerates recovery to the OCP^O state^{29–31}. Binding of FRP occurs to the CTD, most likely at a site covered in OCP^O by the α A-helix, although some secondary, as yet unidentified, site might exist on the NTD or the interdomain linker too, in order to enable the reversion of domain separation and back-sliding of the carotenoid cofactor into its initial position^{22,32}. Spectral and structural changes of the protein and the carotenoid upon photoexcitation have been studied by multiple spectroscopic approaches^{14,28,33,34}; however, main spectral and structural intermediates within the OCP photocycle (if existent) are still elusive, as it is the case for the atomic structure of the most important, biologically active OCP^R state.

The photocycle of OCP was previously studied with a time resolution of up to 100 ms by many scientific groups including ours. Such experiments are usually applied for determining the rate constant of the OCP^R to OCP^O transition, which is often considered as the rate constant of protein refolding. Femtosecond (fs) time-resolved absorption spectroscopy has been used to probe the initial events following photoexcitation and excited state dynamics covering the time scale up to nanoseconds, and has revealed short-lived far-red-shifted absorption spectra, which have frequently been discussed as bearing similarities to internal charge transfer (ICT) states^{2,34,35}. The ultra-fast (fs) transitions between the excited states of the OCP chromophore were studied for several OCP species revealing that in both, orange and red, states the ECN cofactor has a very short (~6 ps) excited state lifetime indicating that both states are potentially suitable for dissipation of excitation energy of PBs. Thus, the conformation of the protein matrix, but not the spectral state of its chromophore, are crucial for PBs fluorescence quenching^{2,35,36}. Additionally, substitution of Arg-155 to Leu was shown to suppress the induction of fluorescence quenching without a loss of photoactivity¹⁸, and constitutively quenching forms like RCP and the OCP^{W288A} mutant^{17,21} indicate that photoconversion and quenching are discrete events, suggesting that the protein state determines its functionality, while the color of the sample is only a side effect. Since the rate constants of protein motions are significantly slower than the fs transients, the physiologically relevant OCP state capable of PBs fluorescence quenching should appear when the carotenoid is already back in the ground state, while between 100 ms and 1 s, there is already a decay of the red state due to back-relaxation and refolding of the protein.

Raman spectroscopy and theoretical calculations have hinted at the configurational changes of the carotenoid that give rise to spectral shifts, and at the influence of the protein matrix on color tuning^{11,15,33,37}. Photoconversion is apparently accompanied by a reduction of the ring rotation angles at the C6-C7(C6'-C7') single bonds of the carotenoid, which leads to an increase of the apparent conjugation length of the polyene chain, and to a relief of bending tension of the latter. As outlined by the recent study of Bandara and colleagues³⁸, this strained chromophore configuration in the dark-adapted state distinguishes OCP from other photoreceptors, in which strained chromophores are the initial or intermediate photoproducts on the way to the product state. Bending of the chromophore in OCP^O most likely is due to the off-axis H-bond interaction of the 4-keto oxygen to the N-H group of Trp-288 in the CTD, while the carotenoid is otherwise tightly packed by a cavity constriction at the inter-domain interface and mainly hydrophobic and π -stacking interactions with Trp-110 in the NTD. Dynamic X-ray crystallography has identified very early structural intermediates of photoconversion showing detachment of the α A-helix, initial rigid-body separation of the CTD and retraction of Tyr-201 and Trp-288 from the ketolated β -ring, indicating that breaking of the specific chromophore-protein H-bonds is one of the initial triggers of photoconversion³⁸. At the other end of the time scale, in the range of hundreds of milliseconds to hundreds of seconds, spectroscopic monitoring of light-induced absorption or fluorescence changes has revealed the kinetic and thermodynamic aspects of the global phototransformations between OCP^O and OCP^{R11}, as well as the influence of amino acid substitutions, or the action of FRP on these processes^{20–22}. However, there is still a large time window to be covered by time-resolved absorption and other spectroscopic techniques in order to elucidate processes occurring between hundreds of nanoseconds to milliseconds for resolving the intermediate states of OCP, which appear during the photocycle. This previously omitted time window spans many orders of magnitude after photoexcitation, when the chromophore has for long returned to the electronic ground state, preceding the dramatic conformational changes of the protein, which occur upon photoactivation and back-relaxation. Importantly, this range of timescales (10^{-7} – 10^{-3} s) has been demonstrated to be crucial for the photocycle of other photoactive proteins^{39–41}, and frequently comprises transitions between several intermediate states.

In this paper, we made use of flash photolysis and picosecond fluorescence spectroscopy techniques to reveal novel red and orange intermediate states of OCP characterized by distinct spectroscopic features, which appear during phototransformation to the OCP^R product state and back-relaxation to the dark-adapted OCP^O state.

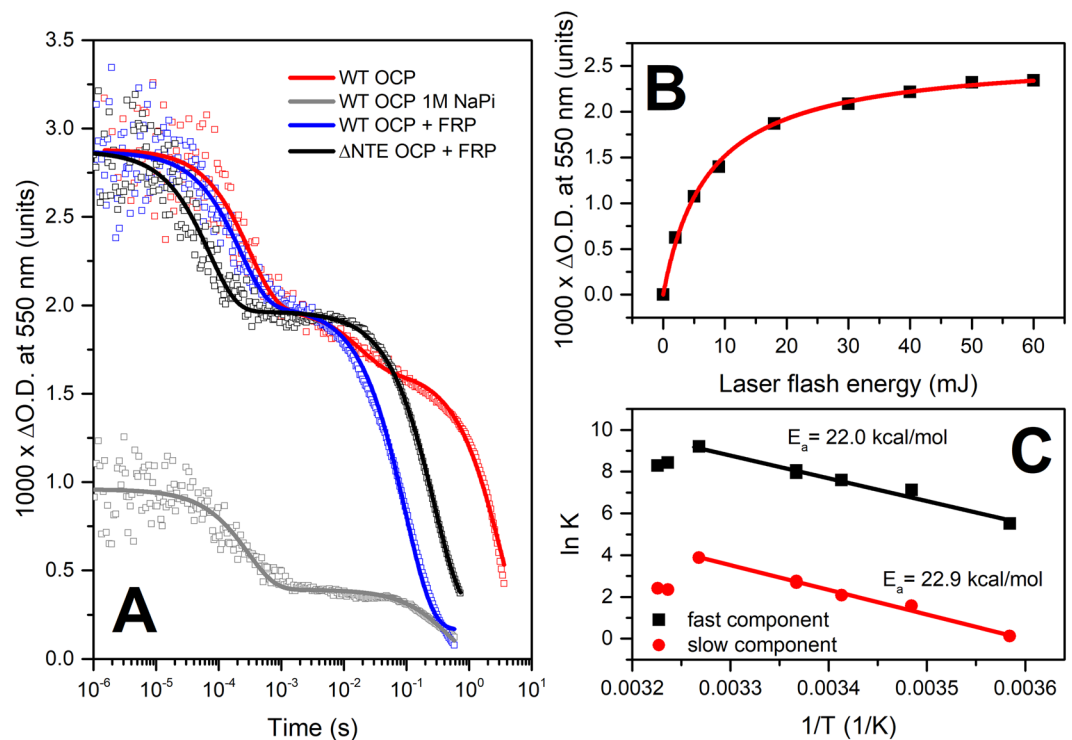


Figure 1. (A) flash-induced transitions of OCP absorption at 550 nm approximated by multiexponential decay: OCP⁰ – red, OCP in 1 M phosphate – grey; OCP in the presence of FRP (1/1.6 concentration ratio) – blue; Δ NTE OCP in the presence of FRP (1/1.6 concentration ratio) – black. Note the logarithmic timescale covering almost 7 orders of magnitude. (B) dependency of the photoconversion amplitude on the energy of the laser flash for OCP in the presence of FRP (1/1.6 concentration ratio). (C) Arrhenius plot of the fast (C1) and the slow (C3) components' rate constants of absorption changes of OCP in the presence of FRP. Experiments were conducted in the range of temperatures from 6 to 37 °C.

These findings result in a more comprehensive and complete photocycle model of OCP with implications on its biological function and regulatory interactions relevant for the role of the protein *in vivo*.

Results and Discussion

Single flash-induced absorption transients of OCP reveal a red intermediate state. First of all, our transient absorption experiments (Fig. 1) show that after irradiation of the sample with a 7-ns laser flash, the increase of OCP absorption at 550 nm (i.e. the spectral red shift) occurs faster than 200 ns, which is the time resolution of our instrument. This remarkable feature indicates that only small changes of chromophore–protein interactions are necessary for the spectral conversion of OCP⁰ to a state with red-shifted chromophore absorption. Namely, 200 ns after photon absorption, the spectral characteristics of OCP are already similar to those of OCP^R, but the protein state could still be significantly different from the physiologically active state (i.e. capable of PBs fluorescence quenching). This is based on the assumptions that (1) conformational rearrangements of OCP are necessary for the interaction with the binding site on PBs [16–17, 25–28] and (2) no dramatic structural changes of the protein occur on the time scale below 200 ns.

Importantly, the amplitude of the absorption changes saturated at pulse energies above 30 mJ (Fig. 1B), indicating that all carotenoid molecules were excited. This fact allows calculating the quantum yield of OCP photoconversion to be equal to 0.3% and the yield of OCP^R formation ~0.2%, in excellent agreement with our previous estimations¹¹. Such a low yield of photoconversion is probably related to the fact that activation of PBs quenching is achieved efficiently only at high-intensity solar radiation. If the yield would be higher, OCP photoconversion leading to PBs quenching may occur already under potentially harmless conditions, thus compromising the efficiency of light harvesting. On the other hand, a lower photoconversion yield would reduce the efficiency of photoprotection, so the proper balance between the stability of OCP⁰ and its sensitivity to blue-green light is crucial.

Further changes of the OCP absorption at 550 nm can be described by three exponential decay components with significantly different lifetimes ranging from hundreds of μ s to tens of s (at 36 °C). The time constant of the first (fast, C1) component is equal to 300 μ s, the second (C2) is about 18 ms and the third (C3) one is about 3.3 s (Table 1). It should be noted that the characteristic rate constant of the slow C3 component has the same order of magnitude as the R-O back-conversion rate, which was determined with a 100 ms resolution technique ($\sim(9\text{ s})^{-1}$) at the same temperature^{11,21}.

In order to further investigate the origin of the two faster C1 and C2 components in the transient absorption decay, we tested several factors affecting the rates of photoconversion, such as the effect of FRP, temperature and high concentrations of phosphate, with the latter expected to act as a kosmotrope and stabilize the OCP⁰

Sample	Fast component (C1)		Intermediate component (C2)		Slow component (C3)	
	$t_1, \mu\text{s}$	$a_1, \%$	t_2, ms	$a_2, \%$	t_3, ms	$a_3, \%$
OCP	300 ± 20	31	18 ± 3	12	3300 ± 100	57
OCP in 1 M NaPi	295 ± 20	59	—	—	430 ± 50	41
OCP + FRP	220 ± 20	32	—	—	95 ± 5	68
$\Delta\text{NTE OCP} + \text{FRP}$	70.4 ± 4	24	—	—	272 ± 20	76

Table 1. Results of approximations of flash-induced absorption transients of OCP by multiexponential decays, as shown in Fig. 1A. All experiments were conducted at 36 °C. The FRP to OCP (or $\Delta\text{NTE OCP}$) concentration ratio was equal to 1.6.

state⁴². Addition of FRP slightly increased the rate constant of C1 to $(220 \mu\text{s})^{-1}$, the C2 component vanished, and the rate constant of C3 was significantly increased up to $\sim(95 \text{ms})^{-1}$. Importantly, the increase of the rate constants in the presence of FRP enabled us to reduce the integration time to solve the principal problem of such time-resolved experiments, which require the accumulation of hundreds and thousands of kinetics traces, i.e., several days of continuous measurements. Addition of FRP also made it possible to accurately measure the temperature dependency (Fig. 1 and Supplementary Figure 1) of these rate constants and to estimate the corresponding activation energies, which appeared to be almost identical for the C1 and C3 components ($\sim 22 \text{ kcal/mol}$, see Fig. 1C). The similarity of the activation energies indicates that the huge differences in the rate constants of C1 and C3 are due to the pre-exponential factor in the Arrhenius law, which reflects the probability of product formation in each of the elementary steps. Thus, the fastest C1 and the slowest C3 components reflect two different states with red-shifted absorption spectrum, for which relaxation to the orange state is characterized by different numbers of attempts (or “collisions” in collision theory) necessary to restore spectral characteristics of OCP^{O} . One may assume that this is due to the protein conformation of OCP at different stages of photoconversion: the protein conformation of the fast-decaying red intermediate (further OCP^{RI}) is probably very similar to that of OCP^{O} (small number of attempts to reach the initial OCP^{O} state), while the slow decay is a feature of the commonly recognized OCP^{R} state with separated structural domains (very high number of attempts to produce OCP^{O}). Assuming that domain separation and the 12-Å carotenoid translocation into the NTD correctly describe the physiologically active OCP^{R} state, as inferred from crystal structures²⁶ and resonance energy transfer measurements²⁸, the slow component reflects the fact that the carotenoid needs to penetrate into the CTD again in order to recover its orange absorption spectrum. Thus, spatial separation of CTD and NTD significantly reduces the probability of back-conversion to the stable OCP^{O} state. The intermediate component C2, which vanishes upon addition of FRP (see below), is not further considered here. It could be associated with an OCP configuration, in which the process of domain separation has just started.

In order to test how the separation of domains affects the yields and lifetimes of different OCP intermediates with red-shifted absorption, we used the non-specific action of high concentrations of inorganic phosphate, a well-known kosmotrope, which is always present in buffers for experiments with PBs, thereby affecting the results of every *in vitro* fluorescence quenching experiment^{16,24}. We found that phosphate significantly reduces the amplitude of flash-induced spectral changes at 550 nm, accelerates the slow C3 component (Table 1) and simultaneously reduces its yield (Fig. 1). This observation indicates that high concentrations of phosphate hinder domain separation of OCP, which is manifested by its accelerated back-conversion, and, therefore, accumulation of the physiologically active OCP^{R} state, which explains why *in vitro* PBs quenching occurs only at a huge excess of OCP ($\sim 40\text{--}100 \text{ OCP}$ per 1 PBs^{16,21,23,24}).

At the same time, addition of phosphate does not affect the C1 component’s decay, thus confirming that the corresponding short-lived OCP^{RI} intermediate, in terms of protein structure, still resembles the compact and stable OCP^{O} state, and its formation does not require significant conformational rearrangements. In contrast to the effect of phosphate, the rate constant of C1 is slightly increased by addition of FRP. This effect is relatively small ($\sim 10\%$) compared to the influence of FRP on the C3 component (Table 1), indicating that FRP interacts effectively with the physiologically relevant OCP^{R} state, but interactions with the red absorbing state that still resembles OCP^{O} -like structural features of the protein are also possible. This conclusion is in agreement with our previous results about the OCP interaction with FRP²¹. Next, deletion of the OCP^{O} -stabilizing N-terminal extension (NTE), which was recently suggested to cover the FRP binding site on the CTD of OCP^{O} , results in formation of stable FRP-OCP complex even in the dark²². In such complexes, the rate constant of the C1 component is at least four times faster compared to full-length OCP and three times faster compared to full-length OCP in the presence of FRP (Table 1). Thus, FRP increases the probability of OCP^{O} state restoration not only from the physiologically active OCP^{R} state, but also from the intermediate red OCP^{RI} state. These facts indicate that in the intermediate OCP^{RI} , the αA helix of the NTE could already be detached from the CTD uncovering the FRP binding site²². However, other possibilities need to be considered as well: (1) The lifetime of the OCP-FRP complex may exceed the intervals between the excitation laser pulses in our experiment (1 s), which results in accumulation of the complex, and (2) binding of FRP occurs even to OCP in the orange state, which was previously observed at high protein concentrations^{21,32}. Although we support the idea of a secondary FRP binding site in the NTD of OCP^{O} , it seems reasonable to assume that the mechanism of FRP action is not simply limited to coupling of the OCP domains. If this were the case, we would expect to see a reduction of the yield of the slow component for $\Delta\text{NTE OCP}$ in the presence of FRP, as observed in experiments with phosphate; however, our data indicate that strong binding of FRP to $\Delta\text{NTE OCP}$ does not prohibit formation of the OCP^{R} state with separated domains (Fig. 1).

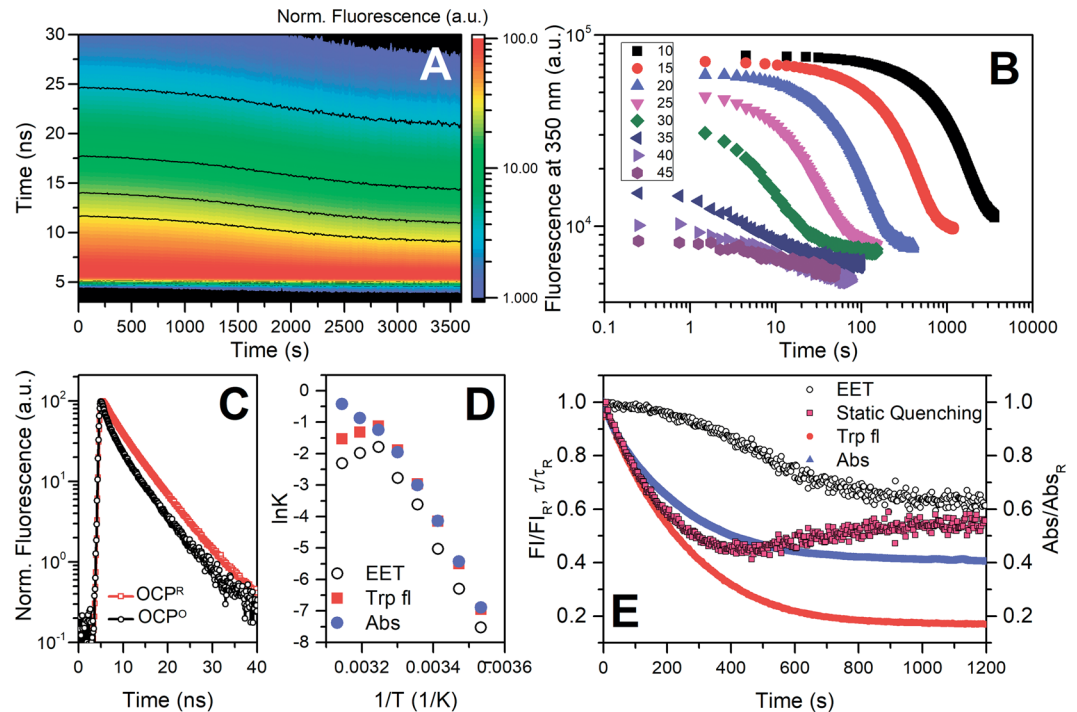


Figure 2. Changes of intrinsic Trp fluorescence of OCP associated with OCP^R-OCP^O conversion. **(A)** a typical set of 400 fluorescence decay kinetics normalized to maximum intensity measured at 10 °C successively after switching off the actinic light, causing conversion of OCP from the red to the orange form. Black lines indicate the levels of fluorescence intensity. **(B)** time courses of fluorescence intensity changes at 350 nm upon the OCP^R-OCP^O transition at temperatures indicated by different colors as described in the inset (values in °C). Each experimental point was obtained by integration of the corresponding Trp fluorescence decay curve. Note the logarithmic scales of both axes. **(C)** normalized Trp fluorescence decay kinetics of the photoactivated (OCP^R) and back-converted (OCP^O, after 60 minutes in the dark) protein. The experiment was conducted at 15 °C. **(D)** Arrhenius plots for the OCP^R-OCP^O relaxation measured as absorption changes at 550 nm (Abs, blue circles), changes of Trp fluorescence intensity (Trp fl, red squares) and changes of average Trp fluorescence lifetime (EET, open circles) calculated from the data presented in **(B)**. **(E)** characteristic time courses of OCP^R-OCP^O transitions of OCP measured as changes of carotenoprotein absorption (blue) at 550 nm, and Trp fluorescence intensity (red circles) and lifetime (or EET, open circles) at 350 nm. Transitions were measured at 15 °C, the concentration of the sample was identical for fluorescence and absorption measurements. The values of O.D., fluorescence intensity and lifetimes were normalized to unity. The time-course of the static quenching (red squares) was calculated from the changes of overall fluorescence intensity $\frac{F(t)}{F_R}$ and average lifetimes $\frac{\tau(t)}{\tau_R}$ as $\frac{Q(t)}{Q_R} = 1 - \frac{\tau(t)}{\tau_R} + \frac{F(t)}{F_R}$ ⁴⁴.

Intrinsic fluorescence of OCP reveals an orange intermediate state. Considering the lifetimes of OCP^R and OCP^O states (~300 μs and 3.3 s, respectively, see Table 1), it is clear that continuous (or high frequency) excitation of the sample by actinic light leads to accumulation of physiologically active OCP^R state. The kinetics of back-relaxation of this state to OCP^O was previously studied in detail, but from the perspective of the chromophore absorption spectrum only. Previously, we showed that the OCP photocycle can be studied by different fluorescence techniques^{14,28,43}, including the monitoring of Trp fluorescence¹¹. Thus, we decided to follow the intrinsic fluorescence of OCP and compare the kinetics of carotenoid- and protein-related transients. For this purpose, we used the same samples and experimental settings as described above to measure the kinetics of OCP^R to OCP^O relaxation. Namely, (i) changes of absorption at 550 nm and (ii) Trp fluorescence emission at 350 nm were studied. Fluorescence was detected by time-correlated single photon counting, which allowed us to assess not only the changes of fluorescence intensity, but also the lifetime(s) of Trp fluorescence. After photoconversion of the sample into the OCP^R state (1 min of actinic light illumination), the actinic light was turned off and a sequence of picosecond-resolved fluorescence decay kinetics was recorded (Fig. 2A). We found that Trp fluorescence intensity was significantly (up to 85%) quenched in the dark-adapted OCP^O state compared to the situation in OCP^R. However, the corresponding differences of average fluorescence lifetime were less than 40% (Fig. 2C). If we roughly assume that in the red state, all five Trp residues emit fluorescence with the same quantum yield, and overall quenching is a combination of static quenching and excitation energy transfer (EET) proportional to number of residues involved in each type of quenching, one may calculate that in the orange state, only one Trp residue (of five) may transfer excitation energy to the carotenoid via Förster resonance energy transfer (resulting in $1/5 \times 60\% = 12\%$ of total possible intensity), while the other four residues are fully quenched statically due to ground state interactions with the carotenoid or other amino acids (resulting in zero contribution to total intensity). Thus, the observed reduction of Trp fluorescence intensity by 85% is reasonable. The residues involved in static quenching are most likely directly involved in protein-chromophore interactions, such as Trp-288 (H-bond

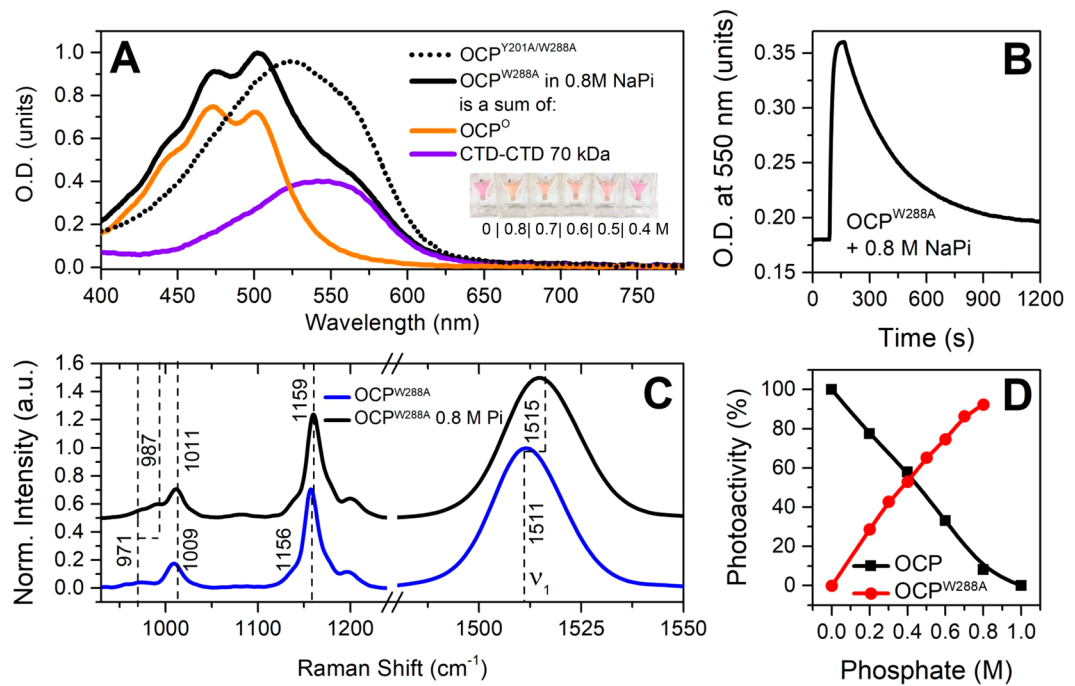


Figure 3. Effects of phosphate on OCP^{W288A}. **(A)** absorption spectrum of OCP^{W288A} in 0.8 M phosphate buffer. The spectrum represents a mixture of orange and violet forms. The dotted line shows the absorption spectrum of the OCP^{Y201A/W288A} mutant, which is identical to the initially purple OCP^{W288A}, but not sensitive to phosphate. The inset shows images of cuvettes containing solutions of OCP^{W288A} in buffers with different phosphate concentration (indicated). **(B)** photocycle of OCP^{W288A} measured as changes of O.D. at 550 nm upon illumination by actinic light. **(C)** Raman spectra of OCP^{W288A} without and with phosphate. **(D)** photoactivity of wild-type OCP and the OCP^{W288A} mutant at different phosphate concentrations. Photoactivity was determined as changes of O.D. at 550 nm normalized to the carotenoid concentration in the sample. Maximum changes of O.D. at 550 nm for wild-type OCP in the absence of phosphate were set to 100%.

to carotenoid), Trp-110 (π -stacking with carotenoid), and Trp-41, or residues involved in inter-domain interactions such as Trp-277, since it forms an H-bond to Asn-104, as inferred from the crystal structures (see the OCP structure overview in Fig. 4A).

Analysis of the time courses of absorption and fluorescence changes upon back-conversion of OCP^R to OCP^O revealed that changes of Trp fluorescence lifetimes occur significantly slower than the overall changes in fluorescence intensity, whereas the rate constants of the latter were similar to those of re-formation of the orange state monitored by absorption changes at 550 nm (Fig. 2D). This fact indicates that restoration of the initial EET efficiency between Trp residues and the carotenoid, as characteristic for the dark-adapted OCP^O state, occurs only after the protein-carotenoid system is already in its orange form. On the other hand, the comparison of the changes of fluorescence lifetimes and intensities allows discriminating between dynamic (EET-related) and static quenching (Fig. 2E). Our data show that restoration of static quenching (e.g. due to H-bond formation or other interactions of Trp residues) precedes the changes in carotenoid-protein absorption. We postulate that formation of this distinct orange intermediate (further termed OCP^{O1}) precedes the final structural rearrangements and restoration of protein-chromophore interactions, which are necessary for stabilization of CTD-NTD interactions and formation of the initial OCP^O state. Considering that restoration of the orange absorption spectrum of the carotenoid requires its correct positioning between OCP-CTD and -NTD including the formation of H-bonds and eventually also the characteristically bent structure of the polyene chain, we assume that relocation of carotenoid from NTD to CTD is a primary step on the way to the dark-adapted, stable OCP^O. As discussed earlier, the rate of OCP^R-OCP^O back-conversion depends on multiple factors; however, the re-establishment of the critical H-bonds between the keto oxygen on the β -ring of ECN and Trp-288 and Tyr-201 must be crucial for stabilization of the OCP^{O1} intermediate state and the following formation of OCP^O.

Roles of Trp-288 and Tyr-201 in protein-carotenoid interactions and stabilization of the orange form.

Previously, we characterized the purple W288A mutant of OCP, which appeared to be functionally similar to the physiologically active OCP^R state in terms of capability of PBs fluorescence quenching and interaction with FRP^{14,21}. Upon addition of FRP to OCP^{W288A} we observed complex formation with 1:1 stoichiometry, and the absorption spectrum of this complex exhibited characteristic signatures of the orange state (referred to as “orangeing”), presumably due to OCP^{W288A} stabilization by FRP²¹. Here we hypothesized whether the FRP-induced stabilization of OCP^{W288A} can be mimicked by kosmotropic phosphate anions, which act non-specifically^{19,24,42,45}, resulting in stabilization of CTD-NTD interactions (see Fig. 1 and description in text). Increasing the phosphate concentration in OCP^{W288A} solutions (pH was kept constant) caused a gradual increase of absorption in the blue

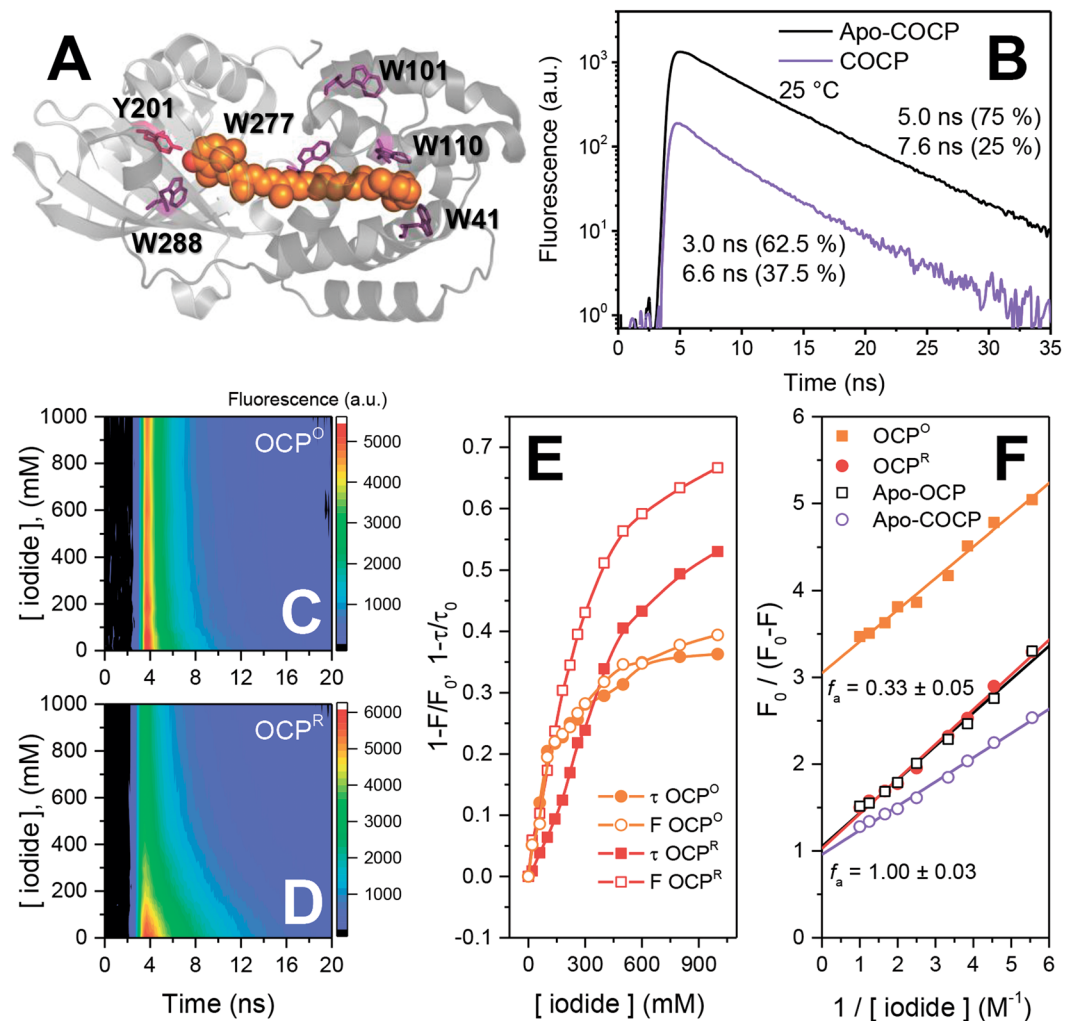


Figure 4. Quenching of Trp fluorescence in OCP and COCP by the carotenoid cofactor and iodide. (A) location of all Trp residues and Tyr-201 in the crystal structure of OCP in the orange state (PDB:3MG1). The carotenoid is shown by orange spheres, Trp residues and Tyr-201 are shown as violet and pink sticks, respectively. (B) fluorescence decay kinetics of COCP (violet) and Apo-COCP (black) measured at 25 °C. The protein concentrations were equal in both samples. (C,D) quenching of OCP^O and OCP^R Trp fluorescence by increasing concentrations of iodide. At each iodide concentration, picosecond fluorescence decays were measured. All experiments with iodide were carried out at 2 °C in order to reduce the rate of OCP^R to OCP^O back-conversion. (E) dependencies of quenching efficiency on iodide concentration calculated as changes of fluorescence intensities and average lifetimes from the data presented in panels C and D. (F) modified Stern-Volmer plots of Trp fluorescence quenching by iodide approximated by linear functions. The ordinate intercepts define the reciprocal values of the fraction of accessible Trp residues (f_a). The protein concentrations were equal in all samples.

spectral region and the appearance of vibronic substructure, a characteristic signature of the orange OCP form. Surprisingly, at 0.8 M phosphate, the spectrum of OCP^{W288A} barely retained features of its initial (phosphate-free) state (red-purple, with maximum at 520 nm^{14,21}), and could fairly well be modeled by a sum of two OCP forms (Fig. 3A): an orange OCP^O spectrum (~75%) and a violet spectrum with maximum absorption at 550 nm (25%). Recently, we have demonstrated that the latter violet forms of OCP may appear upon carotenoid (canthaxanthin, CAN) transfer into Apo-OCP⁴⁶ and represent dimers of OCP, in which a symmetric CAN molecule with keto oxygens at both β -rings is symmetrically positioned between two CTDs, as e.g. in the dimeric C-terminal OCP-related Carotenoid-binding Protein (COCP) characterized earlier¹⁵. Such dimers may be additionally stabilized by cross-protein interactions of NTEs and CTDs³⁸. Formation of such violet forms requires intermediates, in which the carotenoid is positioned in the CTD. Therefore, translocation of the carotenoid from the NTD must occur. We assume that only CAN-coordinating species could be stabilized between two CTDs due to the required symmetry of keto/H-bond interactions. These facts strongly indicate that positioning of the carotenoid in OCP^R is not static, and it can move or slide until specific H-bonds with Trp-288 and Tyr-201 are restored, probably after multiple trials. Due to the absence of the H-bond donor Trp-288, the OCP^{OI} state of the OCP^{W288A} mutant is less stable, but this dynamic equilibrium between OCP^{OI} and OCP^R could be shifted towards the orange form by FRP or phosphate, and most likely kosmotropes in general. In the presence of such stabilizing agents, one H-bond

with Tyr-201 is sufficient to preserve OCP in the orange-like state. However, neither FRP nor phosphate affect the absorption spectrum of the OCP^{Y201A/W288A} double mutant (shown in Fig. 3A), which is similar to such of OCP^{W288A}, indicating that in both mutants the carotenoid is not tightly connected to the CTD. It cannot be concluded that the structure of such a phosphate-induced orange-like OCP^{W288A} is identical to OCP^O, but, surprisingly, phosphate does not only restore several of its spectral characteristics, but also the ability to photoconvert under actinic light (Fig. 3B). This fact is also supported by Raman spectra (Fig. 3C), which simultaneously exhibit typical features of violet and red OCP forms, but not of the orange state, because it is inevitably photoactivated by a 532-nm laser used for Raman spectroscopy. Amazingly, the amplitude of photoconversion in this special case is not reduced by the high phosphate concentration (Fig. 3D). Rather, the rates of the red to orange back-conversion were inversely proportional to the phosphate concentration (Supplementary Figure 3). These facts demonstrate that Trp-288 is not necessary for the photoswitching of OCP itself, but that it rather is important for the stabilization of the OCP^{OI} intermediate during back-conversion, or for the formation of the final compact OCP^O state with its distinct carotenoid curvature, as recently outlined by Bandara *et al.*³⁸.

Assignment of tryptophan residues of OCP involved in static and dynamic quenching. The presence of multiple tryptophan residues in OCP (see Fig. 4A) makes discrimination of their fluorescence properties complicated. This issue cannot be directly solved by mutagenesis due to the significance of Trp residues (in particular, Trp-288, Trp-110 and Trp-41) for functional activity of OCP^{18,19}. It is known that excited-state electron transfer to protein backbone carbonyls is the most important mechanism of Trp fluorescence quenching⁴⁷. Considering this fact and the tight interactions between Trp-288 and the keto oxygen of the β -ring of ECN, we assume that the fluorescence of Trp-288 could be statically quenched (see above). In our previous work, we have demonstrated that two CTDs of OCP can bind CAN (with keto oxygens at each β -ring) and that Trp-288 plays an important role in stabilization of this homodimeric COCP^{15,46}. Comparison of the Trp fluorescence decay kinetics of COCP and its apoprotein form (Apo-COCP), both having only two tryptophans (Trp-277 and Trp-288 in the CTD of *Synechocystis* OCP) reveals that the fluorescence of both Trp residues is significantly quenched by about 85% in the presence of the carotenoid (Fig. 4B). Trp fluorescence quenching in COCP is of mixed type, with about 25% dynamic (attributable to the change in average lifetime) and the other about 60% due to static quenching, which means that in the carotenoid-coordinating homodimer of CTDs, two Trps are statically quenched and the other two contribute to EET to the carotenoid. We assume that Trp-288 is statically quenched due to H-bonding with the carotenoid and Trp-277 is quenched due to EET. The situation for Trp-277 in COCP might well be different from the one in the OCP^O state, because in the latter, Trp-277 could be involved in static quenching, since it forms an H-bond to Asn-104 according to the crystal structure¹⁸, but there is no evidence yet for a similar H-bond in the COCP dimer of CTDs.

For further assignment of the mechanism of Trp fluorescence quenching in OCP, we studied Trp fluorescence in the presence of different concentrations of iodide, a well-known and commonly used collisional (dynamic) quencher. Our idea was to compare the iodide-induced quenching mechanism in different protein forms in order to deduce information about the accessibility of different Trp residues in various OCP states. We found that iodide differently affected the fluorescence decay of OCP in its orange and red forms (Fig. 4C,D and E). While Trp fluorescence quenching of OCP^O could be fairly described by the changes in quantum yield, we found a discrepancy between the changes in lifetimes and fluorescence intensity for OCP^R in the presence of iodide, indicating that different types of Trp residues are involved in quenching. In general, the Stern-Volmer plots (fluorescence amplitude ratio F_0/F versus iodide concentration⁴⁴) for Apo-COCP, Apo-OCP and OCP^R were linear up to 500 mM iodide, with the largest slope observed for Apo-COCP (quenching constant of about 4.5 M^{-1}). Essentially coinciding curves with smaller slopes (Stern-Volmer constants of about 3.5 M^{-1}) were determined for Apo-OCP and OCP^R (see Supplementary Figure 4). However, the Stern-Volmer plot of OCP^O showed only very limited quenching by iodide with saturating behavior at low iodide concentrations (Supplementary Figure 4). This observation suggests a substantially limited accessibility of Trp residues in OCP^O, which invoked the necessity to evaluate the data according to the modified Stern-Volmer plot ($F_0/(F_0 - F)$ versus $1/[I^-]$, see⁴⁴), as depicted in Fig. 4F, to determine the fraction of accessible Trp residues (f_a) in OCP^O. For OCP^O, the analysis of the modified Stern-Volmer plots yielded a f_a value of about 0.33 (Fig. 4F). It is important to recall that in the compact OCP^O state, up to four out of five Trp residues are already involved in static quenching due to interactions with the carotenoid (see text above), leaving only one Trp residue contributing to the observed fluorescence. Trp-101 is actually close to the surface and apparently accessible to collisional quenching by iodide. Considering the structure of OCP^O (PDB entry: 3MG1), the Trp-101 residue should be the one involved in EET (see above), being farthest from the carotenoid (Fig. 4A), while the Trp residues in the carotenoid-coordinating cavity, Trp-288, Trp-41 and Trp-110 (involved in interactions with the carotenoid) and Trp-277 (H-bond formation to Asn-104) are subject to static quenching. These considerations are in agreement with the character of Trp-277 quenching observed in COCP.

The higher efficiency of Trp quenching in OCP^R compared to OCP^O, as well as for Apo-OCP, which is similarly extended in structure⁴³, and Apo-COCP, is probably due to differences in protein conformation. While OCP^O is highly compact, the red and the other extended states are characterized by domain separation, solvent exposure of the interdomain cavity, and properties of the molten globule state^{11,14}, which all increase the accessibility of tryptophans to iodide.

Conclusions

In this work, we utilized a combination of time-resolved spectroscopic techniques to study the photoconversion and consequent back-relaxation of OCP. This approach allowed us to determine two novel intermediate states of the OCP photocycle, which can clearly be identified by distinct spectroscopic features, in addition to the stable orange OCP^O and the physiologically active red OCP^R states (Fig. 5). We found that accumulation of the red intermediate state OCP^{RI}, which is identical to OCP^R in terms of its absorption spectrum, occurs faster

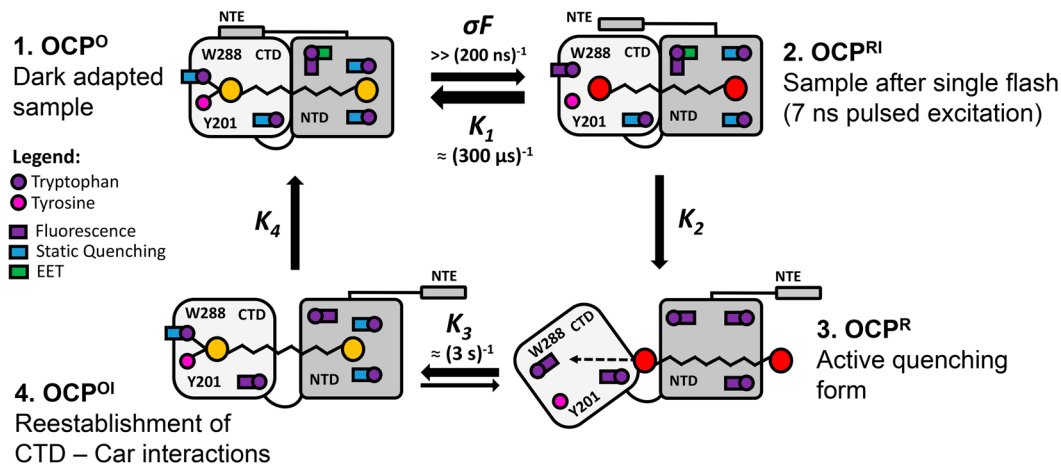


Figure 5. Novel aspects of the OCP photocycle. See text for details.

than 200 ns. We assume that the extremely fast photoisomerization of the carotenoid disrupts hydrogen bonds between the keto oxygen at the β -ring of ECN (or CAN) and Trp-288/Tyr-201 in the CTD of OCP, which affects the absorption of the carotenoid and leads to the first spectral intermediate OCP^{RI} (Fig. 5, state 2). The features of Trp fluorescence of this state need to be studied in more detail, but most probably it is already characterized by increased fluorescence intensity due to at least partial elimination of static quenching. The OCP^{RI} state is probably characterized by a protein conformation similar to the dark-adapted OCP^O, and, thus, is able to rapidly convert into the orange state by “clamping” the chromophore. Conversion into the red OCP^R form is associated with a fast relaxation of the initially bent carotenoid, which, acting just as a spring, may push the protein towards conformational rearrangements including detachment of the α A helix of the NTE³⁸. This reduces the stability of the CTD-NTD protein-protein interactions and leads to separation of domains. Considering the results of dynamic X-ray scattering and the atomic structures of OCP^O and RCP^{26,38,48}, we may assume that the NTE is acting like a conductor of the signal from the CTD into the NTD, which may trigger small but important rearrangements in the NTD, including the 6° rotation of the α -helix encompassing Trp-41, and thus facilitating the translocation of the carotenoid. In terms of kinetics, the red OCP^R state with separated domains is much more stable compared to the intermediate OCP^{RI}, since the geometry of OCP^R reduces the probability that the carotenoid reaches the CTD again at least 10,000-fold (compare time constants for the OCP^{RI}-OCP^O (300 μ s) and the OCP^R-OCP^O transition (3.3 s)).

Together with the observed kinetic properties of dynamic and static quenching upon back-conversion of OCP^R to OCP^O (Fig. 2E), the determination of Trp residues involved in different types of quenching provides novel insights into carotenoid-protein interactions in the intermediate states. Considering the differences in the rate constants, we postulate that restoration of the initial orange state OCP^O occurs in several steps. First of all, the carotenoid restores its position in the NTD, which probably requires a translocation comparable to 12 Å²⁶. This step does not necessarily affect absorption of the carotenoid-protein system; however, it results in restoration of static quenching of Trp-41 and Trp-110 (Fig. 2E), and is most probably reversible. We assume that the formation of violet states (Fig. 3A) is indicative of significant mobility of the carotenoid in the NTD, which can shift by about 12 Å to its position like in the RCP crystal structure (PDB: 4XB4), but it also can slide in the opposite direction. The second step occurs only if NTD and CTD are properly oriented against each other (likely to be assisted by FRP), so that the carotenoid may reach Tyr-201 and Trp-288 in a correct configuration, resulting in the formation of the intermediate state OCP^{OI}, which is characterized by orange-shifted absorption and static quenching of three Trp residues. Importantly, this state can be reached without the assistance of Trp-288 (see Fig. 3); however, the latter determines the stability of this intermediate. The next and final step towards OCP^O requires adjustments of the protein structure, which result in restoration of the initial EET efficiency from Trp-101 to the carotenoid (Fig. 5), and most likely also involve the final bending of the carotenoid into its strained configuration as seen in the OCP^O crystal structure. These final atomic-scale adjustments of the protein structure probably affect some spectral characteristics of the carotenoid including Raman bands responsible for out-of-plane distortions of the polyene chain due to final compaction of the protein. Thus, a combination of rapid time-resolved spectroscopy approaches, and of infrared spectroscopy in particular, will be indispensable to study such transient species.

Our experiments with the OCP^{W288A} protein revealed that the carotenoid position in the OCP^R state is not confined to only the NTD, and that translocation of the carotenoid from the NTD to CTD may occur spontaneously (see Fig. 3). Conversion into the orange intermediate OCP^{OI} state is initiated by carotenoid translocation towards the CTD, which probably requires restoration of carotenoid β -ring position and hydrophobic interactions with Trp-41 and Trp-110, simultaneously quenching their fluorescence (Fig. 2E). Conversion to the orange absorption spectrum is possible due to restoration of the hydrogen bond to Tyr-201 and can be externally stabilized by FRP or high phosphate concentrations, although natural stabilization of carotenoid in this state requires additional bonding with Trp-288. Stabilization of the OCP^{OI} state induces conformational changes of the protein structure, which follows the changes in absorption spectrum at a slower rate, resulting in the pronounced *asynchrony* of

the photoactivation-induced changes in OCP (Fig. 2E). Thus, it is important to discriminate between spectral characteristics and functional (physiological) properties of different OCP states, the changes of which may occur asynchronously. Considering the well-established fact that the carotenoid is an excellent quencher of excitation energy in both red and orange state, and the importance of the OCP conformation for interactions with other proteins, one can hypothesize that OCP^{OI} state is still capable of PBs fluorescence quenching and interaction with FRP, while in terms of its spectrum, it is already largely resembling the initial orange state. We also predict that some OCP mutants, which could be trapped in the orange state, may bind to the phycobilisomes and may even induce quenching. Investigation of such mutants by a combination of time-resolved methods is mandatory to reveal the structural determinants underlying the photoprotection mechanism of OCP-like proteins in general.

Materials and Methods

Protein purification. Cloning, expression and purification of the 6xHis-tagged *Synechocystis* OCP, OCP lacking the NTE comprising the first 20 amino acids (Δ NTE), and FRP were described previously^{14,21,22}. Holoforms of the 6xHis-tagged OCP were expressed in echinenone and canthaxanthin-producing *Escherichia coli* cells essentially as described before¹⁵. The His-tag was identical in all the protein forms used. All proteins were purified by immobilized metal-affinity and size-exclusion chromatography to electrophoretic homogeneity and stored at 4 °C in the presence of sodium azide.

Steady-state absorption measurements. Absorption spectra were recorded using a Maya2000 Pro (Ocean Optics, USA) spectrometer as described in^{11,21,28}. Upon absorption measurements, a blue light-emitting diode (LED) (M455L3, Thorlabs, USA) with a maximum emission at 455 nm was used for the photoconversion of the samples (further referred to as actinic light for OCP^O \rightarrow OCP^R photoconversion). The temperature of the sample was stabilized by a Peltier-controlled cuvette holder Qpod 2e (Quantum Northwest, USA) with a magnetic stirrer.

Measurements of flash-induced absorption transients. Flash-induced absorption changes were examined with a home-built flash-photolysis system. Photocycle excitation was provided by the second harmonic of a Nd-YAG Q-switched laser LS-2131M (LOTIS TII, Belarus), using 7-ns pulses at 532 nm. A monochromatic beam with 550 nm and 6 nm FWHM, which was obtained with two monochromators (before and after the sample) from a power-stabilized 100 W halogen lamp (OSRAM, Germany), was used for monitoring transient absorption.

Absorption changes were followed by using a 9658 B (Electron Tubes Ltd., UK) photomultiplier with 300-MHz wide-bandwidth amplifier and a 100 MHz Octopus CompuScope 8327 (Gage, Canada) analog-to-digital converter. Five hundred single traces were averaged to achieve a higher signal-to-noise ratio. The duration between flashes was set to be in the range between 1 and 5 s to allow completion of a photocycle. The traces were converted into a quasilogarithmic time scale by using home-made software. The kinetic traces were fit with a sum of exponentials using Mathematica (Wolfram Research, USA) or OriginPro 2015 (Originlab, USA).

Time-Correlated Single-Photon Counting (TCSPC) techniques for tryptophan fluorescence transients.

In all experiments, OCP photoconversion was triggered by a blue LED (M455L3, Thorlabs, USA), which passed through the FB450-40 bandpass filter (Thorlabs, USA). Fluorescence of the samples was excited by picosecond EPLED-280 laser diode (Edinburgh Instruments, Scotland) with maximum emission at 280 nm corrected by a bandpass filter (AHF, Germany), delivering pulses at 10 MHz repetition rate. Fluorescence of samples in the range from 300 to 500 nm was collected at 90° to excitation pulse via a collimation lens coupled to the optical fiber of the 16-channel detector PML-16-C (Becker&Hickl, Germany). Fluorescence was recorded with a time- and wavelength-correlated single photon counting system SPC-150 (Becker&Hickl, Germany) described in²⁸. Thus, series of fluorescence decay kinetics were obtained during different stages of back-conversion of the samples after exposition of the sample to actinic light. The temperature of the sample was stabilized by a Peltier-controlled cuvette holder Qpod 2e (Quantum Northwest, USA) with a magnetic stirrer.

The fluorescence decay curves were approximated by a sum of exponential decay functions with the SPCImage (Becker and Hickl, Germany) software package. To compare different decay curves, we calculated the average decay time according to the expression: $\tau_{av} = \sum_i^n \tau_i a_i$, where τ_i and a_i are the lifetime and the amplitude (normalized to unity: $\sum_i^n a_i = 1$) of the i -th fluorescence decay component. To obtain the time integrated fluorescence intensity, the number of photons in each time channel of kinetics was summed up. All calculations were performed using the Origin 9.1 (OriginLab Corporation, USA).

For steady-state fluorescence emission and fluorescence excitation spectra measurements, a FluoroMax-4 instrument (Horiba Jobin Yvon, Japan-France) was used.

All experiments presented in this work were repeated at least five times.

References

- Rakhimberdieva, M. G., Stadnichuk, I. N., Elanskaya, I. V. & Karapetyan, N. V. Carotenoid-induced quenching of the phycobilisome fluorescence in photosystem II-deficient mutant of *Synechocystis* sp. *FEBS Letters* **574**, 85–88, <https://doi.org/10.1016/j.febslet.2004.07.087> (2004).
- Polívka, T., Kerfeld, C. A., Pascher, T. & Sundström, V. Spectroscopic Properties of the Carotenoid 3'-Hydroxyechinenone in the Orange Carotenoid Protein from the Cyanobacterium *Arthrospira maxima*. *Biochemistry* **44**, 3994–4003, <https://doi.org/10.1021/bi047473t> (2005).
- Wilson, A. *et al.* A Soluble Carotenoid Protein Involved in Phycobilisome-Related Energy Dissipation in Cyanobacteria. *The Plant Cell* **18**, 992–1007, <https://doi.org/10.1105/tpc.105.040121> (2006).

4. Wilson, A. *et al.* A photoactive carotenoid protein acting as light intensity sensor. *Proceedings of the National Academy of Sciences* **105**, 12075–12080, <https://doi.org/10.1073/pnas.0804636105> (2008).
5. Gorbanov, M. Y., Kuzminov, F. I., Fadeev, V. V., Kim, J. D. & Falkowski, P. G. A kinetic model of non-photochemical quenching in cyanobacteria. *Biochim Biophys Acta* **1807**, 1591–1599, <https://doi.org/10.1016/j.bbabi.2011.08.009> (2011).
6. Polivka, T., Chábera, P. & Kerfeld, C. A. Carotenoid–protein interaction alters the S1 energy of hydroxyechinenone in the Orange Carotenoid Protein. *Biochimica et Biophysica Acta (BBA) - Bioenergetics* **1827**, 248–254, <https://doi.org/10.1016/j.bbabi.2012.10.005> (2013).
7. Stadnichuk, I. N. *et al.* Fluorescence quenching of the phycobilisome terminal emitter LCM from the cyanobacterium *Synechocystis* sp. PCC 6803 detected *in vivo* and *in vitro*. *J Photochem Photobiol B* **125**, 137–145, <https://doi.org/10.1016/j.jphoto.2013.05.014> (2013).
8. Maksimov, E. G. *et al.* The time course of non-photochemical quenching in phycobilisomes of *Synechocystis* sp. PCC6803 as revealed by picosecond time-resolved fluorimetry. *Biochim Biophys Acta* **1837**, 1540–1547, <https://doi.org/10.1016/j.bbabi.2014.01.010> (2014).
9. Maksimov, E. G. *et al.* Features of temporal behavior of fluorescence recovery in *Synechocystis* sp. PCC6803. *Photosynth Res* **125**, 167–178, <https://doi.org/10.1007/s11120-015-0124-y> (2015).
10. Kirilovsky, D. & Kerfeld, C. A. The Orange Carotenoid Protein: a blue-green light photoactive protein. *Photochem Photobiol Sci* **12**, 1135–1143, <https://doi.org/10.1039/c3pp25406b> (2013).
11. Maksimov, E. G. *et al.* The Signaling State of Orange Carotenoid Protein. *Biophys J* **109**, 595–607, <https://doi.org/10.1016/j.bpj.2015.06.052> (2015).
12. Boulay, C., Abasova, L., Six, C., Vass, I. & Kirilovsky, D. Occurrence and function of the orange carotenoid protein in photoprotective mechanisms in various cyanobacteria. *Biochim Biophys Acta* **1777**, 1344–1354, <https://doi.org/10.1016/j.bbabi.2008.07.002> (2008).
13. de Carbon Thurotte, C. B. A., Wilson, A., Perreau, F. & Kirilovsky, D. Biosynthesis of soluble carotenoid holoproteins in *Escherichia coli*. *Sci Rep* **5**, 9085, <https://doi.org/10.1038/srep09085> (2015).
14. Maksimov, E. G. *et al.* A comparative study of three signaling forms of the orange carotenoid protein. *Photosynthesis Research* **130**, 389–401, <https://doi.org/10.1007/s11120-016-0272-8> (2016).
15. Moldenhauer, M. *et al.* Assembly of photoactive orange carotenoid protein from its domains unravels a carotenoid shuttle mechanism. *Photosynthesis Research* **133**(1–3), 327–341, <https://doi.org/10.1007/s11120-017-0353-3> (2017).
16. Wilson, A. *et al.* The essential role of the N-terminal domain of the orange carotenoid protein in cyanobacterial photoprotection: importance of a positive charge for phycobilisome binding. *Plant Cell* **24**, 1972–1983, <https://doi.org/10.1105/tpc.112.096909> (2012).
17. Leverenz, R. L. *et al.* Structural and functional modularity of the orange carotenoid protein: distinct roles for the N- and C-terminal domains in cyanobacterial photoprotection. *Plant Cell* **26**, 426–437, <https://doi.org/10.1105/tpc.113.118588> (2014).
18. Wilson, A. *et al.* Structural determinants underlying photoprotection in the photoactive orange carotenoid protein of cyanobacteria. *J Biol Chem* **285**, 18364–18375, <https://doi.org/10.1074/jbc.M110.115709> (2010).
19. Wilson, A., Punginelli, C., Couturier, M., Perreau, F. & Kirilovsky, D. Essential role of two tyrosines and two tryptophans on the photoprotection activity of the Orange Carotenoid Protein. *Biochim Biophys Acta* **1807**, 293–301, <https://doi.org/10.1016/j.bbabi.2010.12.009> (2011).
20. Thurotte, A. *et al.* Regulation of Orange Carotenoid Protein Activity in Cyanobacterial Photoprotection. *Plant Physiol* **169**, 737–747, <https://doi.org/10.1104/pp.15.00843> (2015).
21. Sluchanko, N. N. *et al.* The purple Trp288Ala mutant of *Synechocystis* OCP persistently quenches phycobilisome fluorescence and tightly interacts with FRP. *Biochim Biophys Acta* **1858**, 1–11, <https://doi.org/10.1016/j.bbabi.2016.10.005> (2017).
22. Sluchanko, N. N., Slonimskiy, Y. B., Moldenhauer, M., Friedrich, T. & Maksimov, E. G. Deletion of the short N-terminal extension in OCP reveals the main site for FRP binding. *FEBS Letters* **591**(12), 1667–1676, <https://doi.org/10.1002/1873-3468.12680> (2017).
23. Jallet, D. *et al.* Specificity of the cyanobacterial orange carotenoid protein: influences of orange carotenoid protein and phycobilisome structures. *Plant Physiol* **164**, 790–804, <https://doi.org/10.1104/pp.113.229997> (2014).
24. Shirshin, E. A. *et al.* Biophysical modeling of *in vitro* and *in vivo* processes underlying regulated photoprotective mechanism in cyanobacteria. *Photosynthesis Research* **133**(1–3), 261–271, <https://doi.org/10.1007/s11120-017-0377-8> (2017).
25. Gupta, S. *et al.* Local and global structural drivers for the photoactivation of the orange carotenoid protein. *Proc Natl Acad Sci USA* **112**, E5567–5574, <https://doi.org/10.1073/pnas.1512240112> (2015).
26. Leverenz, R. L. *et al.* A 12 Å carotenoid translocation in a photoswitch associated with cyanobacterial photoprotection. *Science* **348**, 3 (2015).
27. Liu, H. *et al.* Dramatic Domain Rearrangements of the Cyanobacterial Orange Carotenoid Protein upon Photoactivation. *Biochemistry* **55**, 1003–1009, <https://doi.org/10.1021/acs.biochem.6b00013> (2016).
28. Maksimov, E. G. *et al.* Fluorescent Labeling Preserving OCP Photoactivity Reveals Its Reorganization during the Photocycle. *Biophysical Journal* **112**, 46–56, <https://doi.org/10.1016/j.bpj.2016.11.3193> (2017).
29. Boulay, C., Wilson, A., D'Haene, S. & Kirilovsky, D. Identification of a protein required for recovery of full antenna capacity in OCP-related photoprotective mechanism in cyanobacteria. *Proceedings of the National Academy of Sciences of the United States of America* **107**, 11620–11625, <https://doi.org/10.1073/pnas.1002912107> (2010).
30. Gwizdala, M., Wilson, A., Omairi-Nasser, A. & Kirilovsky, D. Characterization of the *Synechocystis* PCC 6803 Fluorescence Recovery Protein involved in photoprotection. *Biochim Biophys Acta* **1827**, 348–354, <https://doi.org/10.1016/j.bbabi.2012.11.001> (2013).
31. Sutter, M. *et al.* Crystal structure of the FRP and identification of the active site for modulation of OCP-mediated photoprotection in cyanobacteria. *Proceedings of the National Academy of Sciences* **110**, 10022–10027, <https://doi.org/10.1073/pnas.1303673110> (2013).
32. Lu, Y. *et al.* A Molecular Mechanism for Nonphotochemical Quenching in Cyanobacteria. *Biochemistry* **56**(22), 2812–2823, <https://doi.org/10.1021/acs.biochem.7b00202> (2017).
33. Kish, E., Pinto, M. M., Kirilovsky, D., Spezia, R. & Robert, B. Echinenone vibrational properties: From solvents to the orange carotenoid protein. *Biochim Biophys Acta* **1847**, 1044–1054, <https://doi.org/10.1016/j.bbabi.2015.05.010> (2015).
34. Slouf, V. *et al.* Ultrafast spectroscopy tracks carotenoid configurations in the orange and red carotenoid proteins from cyanobacteria. *Photosynth Res*, <https://doi.org/10.1007/s11120-016-0302-6> (2016).
35. Chábera, P., Durchan, M., Shih, P. M., Kerfeld, C. A. & Polivka, T. Excited-state properties of the 16kDa red carotenoid protein from *Arthrospira maxima*. *Biochim Biophys Acta* **1807**, 30–35, <https://doi.org/10.1016/j.bbabi.2010.08.013> (2011).
36. Berera, R., Gwizdala, M., van Stokkum, I. H., Kirilovsky, D. & van Grondelle, R. Excited states of the inactive and active forms of the orange carotenoid protein. *J Phys Chem B* **117**, 9121–9128, <https://doi.org/10.1021/jp307420p> (2013).
37. Fujisawa, T., Leverenz, R. L., Nagamine, M., Kerfeld, C. A. & Unno, M. Raman Optical Activity Reveals Carotenoid Photoactivation Events in the Orange Carotenoid Protein in Solution. *Journal of the American Chemical Society* **139**, 10456–10460, <https://doi.org/10.1021/jacs.7b05193> (2017).
38. Bandara, S. *et al.* Photoactivation mechanism of a carotenoid-based photoreceptor. *Proceedings of the National Academy of Sciences*, <https://doi.org/10.1073/pnas.1700956114> (2017).
39. Gorostiza, P. & Isacoff, E. Y. Optical Switches for Remote and Noninvasive Control of Cell Signaling. *Science* **322**, 395–399, <https://doi.org/10.1126/science.1166022> (2008).

40. Hendriks, J. *et al.* Transient Exposure of Hydrophobic Surface in the Photoactive Yellow Protein Monitored with Nile Red. *Biophysical Journal* **82**, 1632–1643, [https://doi.org/10.1016/S0006-3495\(02\)7514-8](https://doi.org/10.1016/S0006-3495(02)7514-8).
41. Sineschekov, V. A. The system of phytochromes: photobiophysics and photobiochemistry *in vivo*. *Membrane & cell biology* **12**, 691–720 (1998).
42. King, J. D., Liu, H., He, G., Orf, G. S. & Blankenship, R. E. Chemical activation of the cyanobacterial orange carotenoid protein. *FEBS Lett* **588**, 4561–4565, <https://doi.org/10.1016/j.febslet.2014.10.024> (2014).
43. Moldenhauer, M. *et al.* Interaction of the signaling state analog and the apoprotein form of the orange carotenoid protein with the fluorescence recovery protein. *Photosynthesis Research* 1–15, <https://doi.org/10.1007/s11120-017-0346-2> (2017).
44. Lakowicz, J. R. *Principles of fluorescence spectroscopy*. (Springer Science & Business Media, 2013).
45. Fayos, R., Pons, M. & Millet, O. On the Origin of the Thermostabilization of Proteins Induced by Sodium Phosphate. *Journal of the American Chemical Society* **127**, 9690–9691, <https://doi.org/10.1021/ja051352e> (2005).
46. Maksimov, E. G. *et al.* The unique protein-to-protein carotenoid transfer mechanism. *Biophysical Journal* **113**(2), 402–414, <https://doi.org/10.1016/j.bpj.2017.06.002> (2017).
47. Alston, R. W. *et al.* Peptide Sequence and Conformation Strongly Influence Tryptophan Fluorescence. *Biophysical Journal* **94**, 2280–2287, <https://doi.org/10.1529/biophysj.107.116921> (2008).
48. Kerfeld, C. A. *et al.* The Crystal Structure of a Cyanobacterial Water-Soluble Carotenoid Binding Protein. *Structure* **11**, 55–65, [https://doi.org/10.1016/S0969-2126\(02\)00936-X](https://doi.org/10.1016/S0969-2126(02)00936-X) (2003).

Acknowledgements

This study was supported by Russian Scientific Foundation project № 17-74-30019. This work was supported by grants from Russian Foundation for Basic Research 15-04-01930a to E.G.M. and 15-29-01167 to V.Z.P. E.G.M. was supported by Dynasty Foundation Fellowship. The reported study was funded by RFBR and Moscow city Government according to the research project № 15-34-70007 «mol_a_mos». T.F. acknowledges the support by the German Federal Ministry of Education and Research (WTZ-RUS grant 01DJ15007) and the German Research Foundation (Cluster of Excellence “Unifying Concepts in Catalysis”).

Author Contributions

E.G.M., N.N.S., T.F., V.Z.P. and A.B.R. designed research; E.G.M., N.N.S., Y.B.S., A.V.S., E.A.Sl., A.M.A.-S., G.V.T., K.E.K., O.V.S. and E.P.L. performed research; E.G.M., T.F., N.N.S., E.A.Sh. and A.B.R. wrote the paper.

Additional Information

Supplementary information accompanies this paper at <https://doi.org/10.1038/s41598-017-15520-4>.

Competing Interests: The authors declare that they have no competing interests.

Publisher's note: Springer Nature remains neutral with regard to jurisdictional claims in published maps and institutional affiliations.



Open Access This article is licensed under a Creative Commons Attribution 4.0 International License, which permits use, sharing, adaptation, distribution and reproduction in any medium or format, as long as you give appropriate credit to the original author(s) and the source, provide a link to the Creative Commons license, and indicate if changes were made. The images or other third party material in this article are included in the article's Creative Commons license, unless indicated otherwise in a credit line to the material. If material is not included in the article's Creative Commons license and your intended use is not permitted by statutory regulation or exceeds the permitted use, you will need to obtain permission directly from the copyright holder. To view a copy of this license, visit <http://creativecommons.org/licenses/by/4.0/>.

© The Author(s) 2017